

Message-Passing Interatomic Potentials Learn Non-Local Electrostatic Interactions

Sungwoo Kang*

Computational Science Research Center, Korea Institute of Science and Technology (KIST),

Seoul, 02792, Republic of Korea

*Email: sung.w.kang@kist.re.kr

ABSTRACT

This work demonstrates that E(3)-equivariant graph neural network interatomic potentials (GNN-IPs) effectively learn non-local electrostatic interactions and charge transfers. Using a toy model with point charges, it is confirmed that GNN-IPs adeptly interpolate and extrapolate electrostatic interactions, independent of geometric coupling. It is also found that the electrostatic energy between an atom pair is distributed among neighboring atoms, rather than localized solely within the two atoms involved. Furthermore, GNN-IPs have proven successful in capturing non-local interactions through charge transfer on density functional theory reference data, as evidenced by comparative analyses of the potential energy surfaces for Au clusters on both MgO and Al-doped MgO substrates.

Machine-learned interatomic potentials (MLIPs), which are machine learning models that predicts energies and forces of given atomic configurations based on the reference quantum mechanical calculation data, have gained much attention due to their speed, linear scalability, and high accuracy.¹ Most MLIP models predict the atomic energy of a given atom using the descriptors based on local environment as input features,²⁻⁴ based on the assumption that the non-local electrostatic interaction is effectively screened beyond a certain cutoff.⁵ However, when it comes to systems involving a weak dielectric constant and large atomic charges, where electrostatic interactions are not screened within the cutoff radius, these conventional models fail to describe the potential energy surfaces (PES) of the system.⁶ (A similar issue can arise in systems involving large van der Waals (vdW) interactions.⁷) To overcome this issue, developments have been made to include non-local electrostatic interactions in conventional MLIPs.⁸⁻¹⁰

Recent developments in graph neural network interatomic potentials (GNN-IPs) demonstrate significant improvements in terms of accuracy, data efficiency, and transferability compared to descriptor-based models.¹¹⁻¹⁴ These models incorporate a message-passing algorithm, suggesting their capability to describe non-local interactions beyond cutoff. Two previous studies specifically explored this attribute of GNN-IPs: Bochkarev et al. showed that GNN-IPs, specifically the ml-ACE and NequIP models, effectively train on the PES of molecules longer than the cutoff distance with considerable partial charges, indicating their ability to learn electrostatic interactions.¹⁵ Nevertheless, the charge distribution of atoms within a molecule is coupled with the structural deformation. Thus, it remains uncertain whether GNN-IPs primarily learn PES based on structural deformations due to induced charges or if they can directly learn electrostatic interactions independently of geometric coupling. Additionally, Nigam et al. demonstrated that the message-passing algorithm can learn electrostatic interactions in random NaCl structures but concluded that

learning electrostatic interactions using the message-passing algorithm is much less effective compared to simply increasing the cutoff.¹⁶ However, this study only tested linear-based models, and it remains unknown how the incorporation of non-linear activations would affect the results. Overall, questions remain regarding the ability of GNN-IPs to model long-range interactions effectively.

This study demonstrates that the GNN-IP, specifically the NequIP model,¹² captures electrostatic interactions effectively within a reasonable model size. Throughout the study, the SevenNet code is employed.¹⁷ Initially, I construct a simple toy model comprising particles with point charges to eliminate the effect of geometric coupling (Fig. 1a). In Configuration Type I, particles with charges of $1e$, $-1e$, $0.5e$, and $-0.5e$ are included. The $1e$ and $-1e$ particles are placed at a specified distance (d), while the $0.5e$ and $-0.5e$ particles are positioned randomly in a non-periodic cell. Only electrostatic energies and forces are applied between particles. Configuration Type II mirrors Type I but omits the $-1e$ particle in each cell.

Initially, the ability of GNN-IPs to interpolate electrostatic forces is tested (Fig. 1b). The NequIP model, with a cutoff radius of 5 \AA , is trained using structures from both Configuration Type I and II, at distances of $4, 6, 8, 10,$ and 12 \AA . Then the test is performed to evaluate the accuracy of the trained model on a newly generated test set by evaluating the differences in forces acting on the $1e$ particles between Configurations I and II ($F_{1e,I}$ and $F_{1e,II}$ respectively), where the ideal value corresponds to k/d^2 (k : Coulomb constant). The model accurately predicts $F_{1e,I} - F_{1e,II}$ in interpolated regions ($d=5, 7, 9,$ and 11 \AA). To assess extrapolation capabilities, I train the model on distances of $4-8 \text{ \AA}$ and test it for $9-12 \text{ \AA}$ (Fig. 1c). The trained model successfully predicts $F_{1e,I} - F_{1e,II}$ in this out-of-distribution region. This suggests that knowledge learned from interactions between $\pm 1e$ and $\pm 0.5e$, as well as between $\pm 0.5e$ particles, is effectively transferred to interactions

between $1e$ and $-1e$. Note that the validation root-mean square errors (RMSEs) for energy and force are 1.6 meV/atom and 0.020 eV/Å for interpolation model, and 1.4 meV/atom and 0.018 eV/Å for extrapolation model.

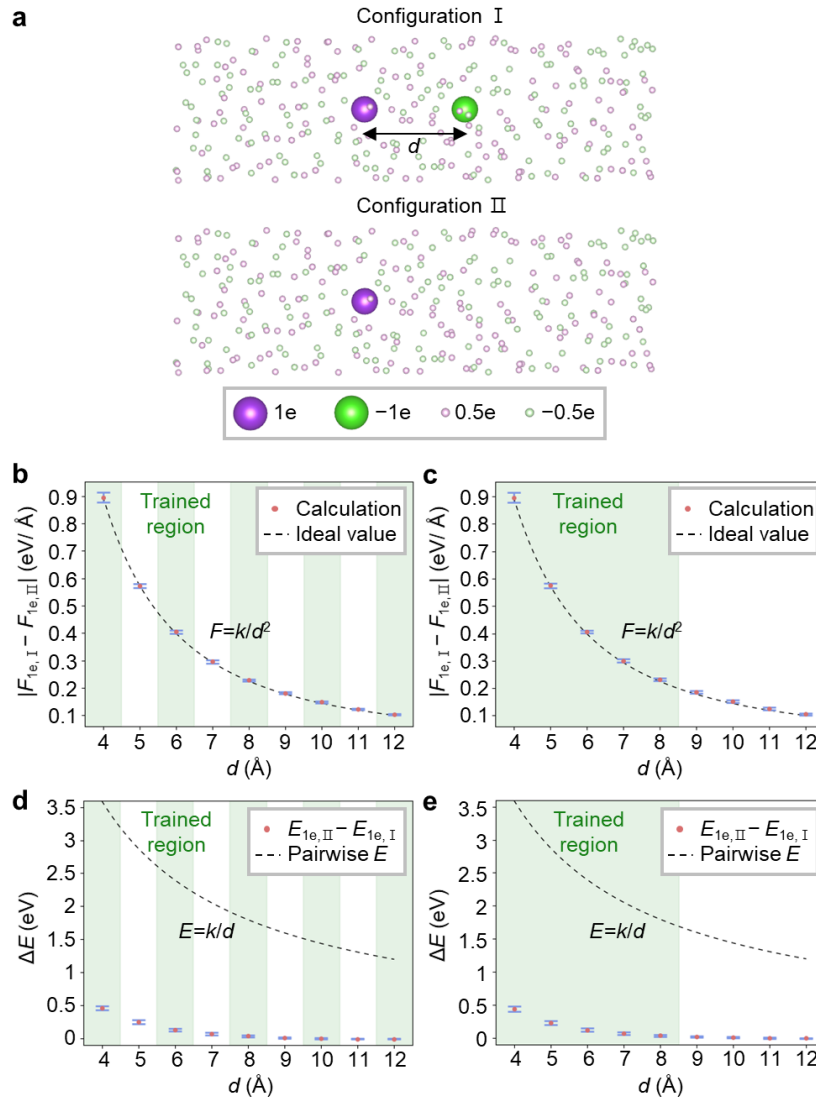


Figure 1 | Test on the toy model. **a**, Schematic illustration of the toy model. Difference in forces acting on $1e$ particle in Configurations I and II for **b**, interpolation test set and **c**, extrapolation test set. The ideal value is plotted as a dotted line ($F=k/d^2$). Error bars represent the standard deviation of the test results. Difference in atomic energy of $1e$ particle in Configuration I and II for **d**, interpolation test set and **e**, extrapolation test set. The absolute value of pairwise electrostatic energy between $1e$ and $-1e$ ($E=k/d$) is plotted in the dotted line. Error bars represent the standard deviation of the test results.

Figs. 1d,e show the atomic energy differences for the 1e particle between Configuration I and II ($E_{1e,I}$ and $E_{1e,II}$, respectively) for interpolation and extrapolation test sets, respectively. The dotted line plots k/d , corresponding to the pairwise electrostatic energy exerted on the 1e particle by the $-1e$ particle. The values of $E_{1e,I} - E_{1e,II}$ values are significantly smaller than the pair-wise electrostatic energy, which indicates that electrostatic energy between an atom pair is distributed among neighboring atoms rather than being localized solely within the two atoms involved. One might assume that this scenario represents a case of ad hoc atomic energy mapping, where atomic energies are inaccurately mapped while total energies are trained accurately.⁵ However, I argue against this being a case of ad hoc mapping, evidenced by the low standard deviation in $E_{1e,I} - E_{1e,II}$ values across varying configurations (Fig. 1d,e), small total-energy errors for test structures (MAE=2.4 meV/atom), and consistent results from independently trained models (interpolation and extrapolation models).

For the next case, Au clusters supported on MgO and on Al-doped MgO, as suggested in ref. 10, are utilized for the model system (Fig. 2a). Doping MgO with Al results in charge transfer from Al to Au, providing a pertinent test case to assess whether GNN-IP can capture charge equilibration beyond the cutoff. In all simulations, the atomic geometries of the supports remain fixed, thus maintaining identical local configurations around the Au clusters. This ensures that geometric coupling effects do not affect the predictions. The NequIP model with cutoff radius of 6 Å is trained on the density functional theory (DFT) calculation data provided in the ref. 10. The RMSE values of energy and force are 2.2 meV/atom and 0.072 eV/Å, respectively.

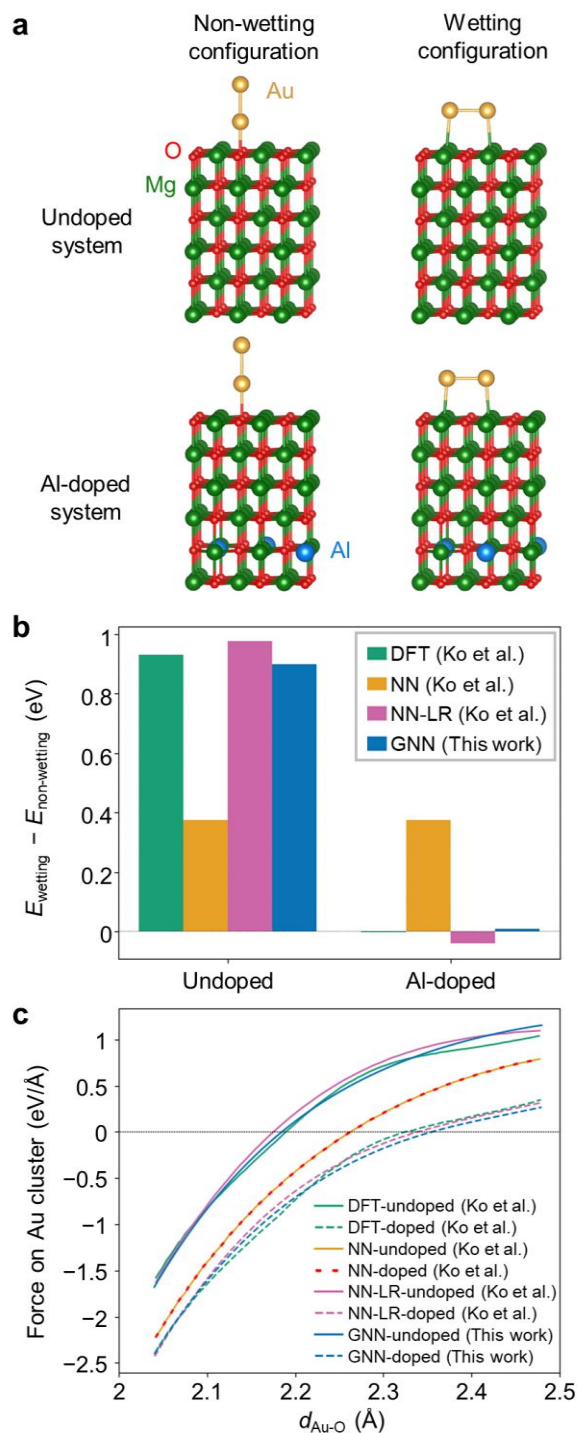


Figure 2 | Test on the DFT reference data with charge transfer. **a**, Atomic configurations of Au clusters in non-wetting and wetting configurations on undoped and Al-doped MgO, respectively. **b**, Energy differences between wetting and non-wetting configurations as calculated by DFT, neural network (NN) potential, NN potential with long-range corrections (NN-LR), and graph neural network (GNN) potential. **c**, Forces acting on Au clusters as a function of the distance between lower Au atom and the nearest O atom in the non-wetting configuration. Results of DFT, NN, and NN-LR are extracted from ref. 10.

Fig. 2b illustrates the energy differences between the wetting and non-wetting configurations for both the MgO and Al-doped MgO systems. The Behler-Parrinello type neural network (NN) model² yields identical energies for both systems, because it fails to distinguish geometric difference beyond the cutoff. The NN model with long-range corrections (NN-LR) offers a more accurate prediction when compared to DFT results, as detailed in ref. 10. This work finds that the GNN-IP (with cutoff distance of 6 Å) accurately predicts the energy differences between non-wetting and wetting configurations, with the slightly smaller error than NN-LR model. The PES of the Au cluster is further explored in Fig. 2c, which depicts the forces acting on the Au cluster in a non-wetting configuration. This analysis is conducted while systematically varying the positions of the Au clusters, keeping the distance between Au atoms fixed at their equilibrium position. The sum of forces on Au atoms is plotted as a function of the distance between the lower Au atom and the nearest O atom. The GNN-IP model successfully replicates the PES of the Au clusters on both MgO and Al-doped MgO supports, demonstrating accuracy comparable to the NN-LR model.

Based on the preceding discussion, I suggest that GNN-IP models can be efficient tools for investigating systems that exhibit non-local interactions due to insufficient screening. However, below considerations must be addressed for further practice: (1) The message-passing algorithm in GNN-IP models, which requires a third atom connecting two others beyond the cutoff, generally functions well in condensed matter systems where atoms are closely interconnected. Nevertheless, in sparser systems like molecular liquids, GNN-IP may encounter challenges in training the PES in this sense. For example, I train the NequIP model on the P₄ molecular liquid dataset in ref. 7 and fail to achieve a reasonable error margin at a practical cutoff (RMSEs of energy and force are

21.5 meV/atom and 0.600 eV/Å, respectively), due to the large intermolecular distances. (2) Technically speaking, the evaluation of electrostatic energy in periodic systems necessitates calculating an infinite sum across all periodic images, typically using methods like Ewald summation. Currently, GNN-IP models are not equipped to perform this calculation. Long-range (>15 Å) electrostatic effects are generally diminished due to effective screening in most condensed matter systems, and the message-passing algorithm presented in this work further reduces the remaining errors in medium-range (10-15 Å) regions. However, careful attention is still required to accurately account for factors such as dielectric screening and the specific charge distribution of each system. Future studies will explore the impact of different model choices, hyperparameters, and test systems to enhance the capabilities of GNN-IP models for learning non-local interactions.

Methods

Toy model

The lattice dimensions of each cell are set to $10 \times 10 \times (24+d)$ Å³, configured in a tetragonal shape. Each cell contains one 1e and one -1e particle, where the coordinates of these particles are set at (5, 5, 12) and (5,5,12+d), respectively, along with $120+5d$ particles each of 0.5e and -0.5e, which are randomly distributed within the simulation cell. The minimum interatomic distance cutoff for the random distribution is set at 1.5 Å. To eliminate periodic effects, 6 Å of vacuum layers are inserted in all directions, which is larger than the cutoff of 5 Å. In total, 200 structures are constructed for each d for training set. The test set used in Fig. 1b-e is generated by the same method as for the training set.

Au-MgO and Au/Al-MgO system

I employ the same training set and test system that are utilized in ref. 10. For the training set, it is stated that random displacements are applied for the configurations in the trajectory shown in Fig. 2c, with standard deviation of 0.02 Å for the substrate atoms, and 0.1 Å for the gold atoms. The half of the training set corresponds to the undoped substrate, and the other half corresponds to the doped substrate. For each substrate configuration, half of the samples were generated with the Au₂ cluster in its wetting configuration, while the remaining half featured the cluster in its non-wetting configuration.

Machine-learned interatomic potentials

The NequIP model is trained using the SevenNet code,¹⁷ and the simulations are performed with the LAMMPS code.¹⁸ The model designed for the point-charge system comprises 5 convolution layers, with a maximum rotation order (l_{\max}) of 3 and 32 features for each rotation order. The model for the Au-MgO system includes 4 convolution layers, with a l_{\max} of 2 and 16 features for each rotation order. For both models, the invariant radial networks utilize a trainable Bessel basis of size 8 and consist of two hidden layers with 64 nodes each, featuring SiLU nonlinearities between the layers. The train/validation sets are split by the ratio of 9:1. Additional details are available in the input files provided in the Supplementary Data.

Data availability

The training and test sets for the toy models are provided in the Supplementary Data. The training set for the Au-MgO system is available in the repository distributed by the previous study of Ko et al.¹⁹ All input files and the trained models are also provided in the Supplementary Data.

Code availability

This study is conducted using the SevenNet code,¹⁷ which is publicly available at <https://github.com/MDIL-SNU/SevenNet>.

References

1. Unke, O. T. *et al.* Machine Learning Force Fields. *Chem. Rev.* **121**, 10142–10186 (2021).
2. Behler, J. & Parrinello, M. Generalized Neural-Network Representation of High-Dimensional Potential-Energy Surfaces. *Phys. Rev. Lett.* **98**, 146401 (2007).
3. Bartók, A. P., Payne, M. C., Kondor, R. & Csányi, G. Gaussian Approximation Potentials: The Accuracy of Quantum Mechanics, without the Electrons. *Phys. Rev. Lett.* **104**, 136403 (2010).
4. Deringer, V. L., Caro, M. A. & Csányi, G. Machine Learning Interatomic Potentials as Emerging Tools for Materials Science. *Adv. Mater.* **31**, 1902765 (2019).
5. Yoo, D. *et al.* Atomic energy mapping of neural network potential. *Phys. Rev. Mater.* **3**, 093802 (2019).
6. Staacke, C. G. *et al.* On the Role of Long-Range Electrostatics in Machine-Learned Interatomic Potentials for Complex Battery Materials. *ACS Appl. Energy Mater.* **4**, 12562–12569 (2021).
7. Deringer, V. L., Caro, M. A. & Csányi, G. A general-purpose machine-learning force field for bulk and nanostructured phosphorus. *Nat. Commun.* **11**, 5461 (2020).
8. Anstine, D. M. & Isayev, O. Machine Learning Interatomic Potentials and Long-Range Physics. *J. Phys. Chem. A* **127**, 2417–2431 (2023).

9. Ghasemi, S. A., Hofstetter, A., Saha, S. & Goedecker, S. Interatomic potentials for ionic systems with density functional accuracy based on charge densities obtained by a neural network. *Phys. Rev. B* **92**, 045131 (2015).
10. Ko, T. W., Finkler, J. A., Goedecker, S. & Behler, J. A fourth-generation high-dimensional neural network potential with accurate electrostatics including non-local charge transfer. *Nat. Commun.* **12**, 398 (2021).
11. Batatia, I., Kovács, D. P., Simm, G. N. C., Ortner, C. & Csányi, G. MACE: Higher Order Equivariant Message Passing Neural Networks for Fast and Accurate Force Fields. Preprint at <https://arxiv.org/abs/2206.07697v2> (2022).
12. Batzner, S. *et al.* E(3)-equivariant graph neural networks for data-efficient and accurate interatomic potentials. *Nat. Commun.* **13**, 2453 (2022).
13. Gasteiger, J., Giri, S., Margraf, J. T. & Günnemann, S. Fast and Uncertainty-Aware Directional Message Passing for Non-Equilibrium Molecules. Preprint at <http://arxiv.org/abs/2011.14115> (2022).
14. Gasteiger, J., Becker, F. & Günnemann, S. GemNet: Universal Directional Graph Neural Networks for Molecules. Preprint at <http://arxiv.org/abs/2106.08903> (2022).
15. Bochkarev, A., Lysogorskiy, Y., Ortner, C., Csányi, G. & Drautz, R. Multilayer atomic cluster expansion for semilocal interactions. *Phys. Rev. Res.* **4**, L042019 (2022).
16. Nigam, J., Pozdnyakov, S., Fraux, G. & Ceriotti, M. Unified theory of atom-centered representations and message-passing machine-learning schemes. *J. Chem. Phys.* **156**, 204115 (2022).

17. Park, Y., Kim, J., Hwang, S. & Han, S. Scalable Parallel Algorithm for Graph Neural Network Interatomic Potentials in Molecular Dynamics Simulations. Preprint at <http://arxiv.org/abs/2402.03789> (2024).
18. Plimpton, S. Fast parallel algorithm for short-range molecular dynamics. *J. Comput. Phys.* **117**, 1–19 (1995).
19. Ko, T. W., Finkler, J. A., Goedecker, S. & Behler, J. A fourth-generation high-dimensional neural network potential with accurate electrostatics including non-local charge transfer. Materials Cloud Archive 2020.X <https://doi.org/10.24435/materialscloud:f3-yh> (2020).

Acknowledgements

This work was supported by the KIST Institutional Project (2E33211).

Author contributions

S.K. designed the study, performed simulations, and wrote the manuscript.

Competing interests

The author declares no competing interests.